MIT Open Access Articles

A microfluidic 3D in vitro model for specificity of breast cancer metastasis to bone

Massachusetts Institute of Technology

A Microfluidic 3D In Vitro Model for Specificity of Breast Cancer Metastasis to Bone

S. Bersini[1,2,+], **J.S. Jeon**[3,+], **G. Dubini**[4], **C. Arrigoni**[5], **S. Chung**[6], **J.L. Charest**[7], **M. Moretti**[2,*], and **R.D. Kamm**[3,8,*]

[1]Department of Electronics, Information and Bioengineering, Politecnico di Milano, Piazza Leonardo da Vinci 32, 20133 Milano, Italy

[2]Cell and Tissue Engineering Lab, IRCCS Istituto Ortopedico Galeazzi, Via R. Galeazzi 4, 20161 Milano, Italy

[3]Department of Mechanical Engineering, Massachusetts Institute of Technology, 77 Massachusetts Avenue, Cambridge, M

[4]Department of Chemistry, Materials and Chemical Engineering, Politecnico di Milano, Piazza Leonardo da Vinci 32, 20133 Milano, Italy

[5]Cell and Tissue Engineering Lab, Gruppo Ospedaliero San Donato Foundation, Milano, Italy

[6]School of Mechanical Engineering, Korea University, Anam-dong, Seongbuk-gu, Seoul, South Korea 136-705

[7]Charles Stark Draper Laboratory, 550 Technology Square, Cambridge, MA, USA 02139

[8]Department of Biological Engineering, Massachusetts Institute of Technology, 77 Massachusetts Avenue, Cambridge, MA, USA 02139

Abstract

Cancer metastases arise following extravasation of circulating tumor cells with certain tumors exhibiting high organ specificity. Here, we developed a 3D microfluidic model to analyze the specificity of human breast cancer metastases to bone, recreating a vascularized bone-mimicking microenvironment with human osteo-differentiated bone marrow-derived mesenchymal stem cells and endothelial cells. The tri-culture system allowed us to study the transendothelial migration of highly metastatic breast cancer cells and to monitor their behavior within the bone-like matrix. Extravasation, quantified 24h after cancer cell injection, was significantly higher in the osteo-cell conditioned microenvironment compared to collagen gel-only matrices (77.5±3.7% vs. 37.6±7.3%), and the migration distance was also significantly greater (50.8±6.2μm vs. 31.8±5.0μm). Extravasated cells proliferated to form micrometastases of various sizes containing 4 to more than 60 cells by day 5. We demonstrated that the breast cancer cell receptor CXCR2 and the bone-secreted chemokine CXCL5 play a major role in the extravasation process, influencing

CORRESPONDING AUTHORS, R.D. Kamm, Department of Biological and Mechanical Engineering, Massachusetts Institute of Technology, 77 Massachusetts Avenue, Cambridge, MA, USA 02139, Phone: (+1) 617 253 6236, rdkamm@mit.edu, M. Moretti, IRCCS Istituto Ortopedico Galeazzi, Via R. Galeazzi 4, 20161 Milano, Italy, Phone: (+39) 02 6621 4061, matteo.moretti@grupposandonato.it.
[+]S.B. and J.S.J. contributed equally to the present work.
[*]M. Moretti and R.D. Kamm equally contributed.

extravasation rate and travelled distance. Our study provides a novel 3D *in vitro* quantitative data on extravasation and micrometastasis generation of breast cancer cells within a bone-mimicking microenvironment and demonstrates the potential value of microfluidic systems to better understand cancer biology and screen for new therapeutics.

Keywords

microfluidics; bone; hydrogel; breast cancer; metastasis; extravasation

1. Introduction

The systemic nature of cancer metastases coupled with the resistance to most current therapeutic agents explains why metastases are responsible for as much as 90% of cancer-related mortality [1, 2]. The dissemination of circulating tumor cells (CTCs) represents a "hidden" process leading to micrometastases where quiescent cells can survive for prolonged periods before their activation [3, 4].

In order to generate secondary tumors, CTCs must survive in the circulation and undergo a process known as extravasation [5–7]. Extravasation into the parenchyma of distant tissues represents a multistep sequence within the metastatic cascade, in which cancer cells establish transient, metastable contacts with the endothelium [8–10], firmly adhere to the vascular walls [11] and finally transmigrate across the endothelial and pericyte layers [12] as microcolonies or isolated cells [13, 14].

Although it is well known that circulatory patterns play a pivotal role in the spread of metastatic cells to secondary sites, the cross-talk between specific cancer cell types and receptive environments also preferentially guides the dissemination process [15]. In this context, it has been shown that breast cancer metastasizes to bone, liver, lung and brain while prostate cancer frequently disseminates to bone [3]. Particularly, autoptic studies have demonstrated that 70% of advanced breast cancer patients have skeletal metastases, leading to pain, due to spinal cord compression and fractures, and often mortality [16, 17].

Despite the clinical importance of metastases, research has largely focused on the oncogenic transformations leading to the development of primary tumors and much remains to be learned about the metastatic process [5]. Moreover, a deeper understanding of the metastatic cascade and particularly of extravasation to a specific organ could promote the development of new therapeutic strategies, thus improving cancer survival rates [12].

In vivo and *ex vivo* models have been developed to study the extravasation process in mice and zebrafish embryos through intravital microscopy [13, 18, 19] and advanced models of bone metastasis employ intravenous, intracardiac or direct skeletal injection of breast cancer cells [20, 21]. Although these experiments replicate physiological conditions, they cannot model all aspects of the interaction and cross-talk between human cancer cells, human endothelial cells and human tissue parenchyma. Moreover, strictly regulated, reproducible parametric studies are difficult to perform.

In vitro models, although unable to fully replicate the *in vivo* situation, can overcome some of these limitations by using human cells throughout and providing highly controllable environments where single culture parameters can be modified [22, 23]. Traditional assays (e.g. Boyden chamber, wound assay, and others) have been widely used to study cell migration in response to chemotactic gradients, particularly cancer cell invasion and

migration. However, they do not provide tight control over the local environment, complex interactions cannot be accurately analyzed, and imaging is limited [24–26].

Microfluidics can provide useful model systems to investigate complex phenomena under combination of multiple controllable biochemical and biophysical microenvironments, coupled with high resolution real time imaging [27–30]. The synthesis of these features is technically impossible with traditional assays as the Boyden chamber [31, 32]. Toward this goal, several microfluidic devices have been developed to investigate cancer cell transition to invasion and migration from a primary site [33–35], cell transition effects across mechanical barriers [36], intravasation [37], adhesion [38] and extravasation [39–44] processes.

However, despite supporting experimental evidence, none of the previously reported *in vitro* systems has reproduced the specific cross-talk among several cell types in a complex cancer microenvironment during extravasation and none have gone beyond the study of transendothelial migration towards a non-organ-specific extracellular matrix (ECM). Indeed, the importance of organ-specific cancer models lies in the possibility to better clarify the mutual interactions between different cell populations in a well-defined microenvironment, in order to develop highly focused and more effective therapies.

We develop here a new tri-culture microfluidic 3D *in vitro* model demonstrating the key role played by an osteo-cell conditioned microenvironment, a collagen gel with embedded osteo-differentiated bone marrow-derived human mesenchymal stem cells (hBM-MSCs) [45] and lined with endothelium, in the extravasation process of highly-metastatic MDA-MB-231 human breast cancer cells [16, 46].

2. Materials and methods

2.1. Microfluidic system

A previously developed microfluidic device consisting of 3 media channels and 4 independent gel channels was adopted in the present study. Specifications and microfabrication details of the system were previously described [47, 48]. Inlet and outlet ports of the PDMS (poly-dimethyl-siloxane; Silgard 184, Dow Chemical) devices were bored using disposable biopsy punches and the PDMS layer was bonded to a cover glass to create microfluidic channels 150 μm deep with oxygen plasma treatment. Eight gel regions (225 μm by 150 μm) interfacing with the central media channel are provided to study cell interactions. The PDMS channels were coated with a PDL (poly-D-lysine hydrobromide; 1 mg/ml; Sigma-Aldrich) solution to promote matrix adhesion. Then, collagen type I (BD Biosciences) solution (6.0 mg/ml) with Phosphate Buffered Saline (PBS; Invitrogen) and 1N NaOH, and embedded with osteo-differentiated hBM-MSCs was injected within the 4 independent gel channels using a 10 μl pipette and incubated for 30 min inside humid chambers to form a hydrogel. A representative schematic of the model is provided in Fig. 1, showing the generated tri-culture system with particular emphasis on the osteo-cell conditioned microenvironment. After 3 days, diluted Matrigel™ (BD Biosciences) solution (3.0 mg/ml) was introduced as a thin layer coating the central media channel; cold medium was injected after 1 min to wash and prevent channel clogging. Endothelial cells were introduced into the central media channel to generate a monolayer covering channel walls and gel-channel interfaces. Cancer cells were injected after 3 additional days in the same channel and transmigration into the osteo-cell conditioned regions was analyzed after 24 h [41]. Additionally, proliferation and clustering of transmigrated cancer cells within the osteo-cell conditioned matrix were studied after 2, 3 and 5 days.

2.2. Cell culture

Bone marrow-derived human mesenchymal stem cells were obtained harvesting whole bone marrow aspirates from patients undergoing hip surgery and selected by plastic adherence according to an optimized protocol [49]. Cells of passage 7 or lower were cultured in osteogenic medium containing L-ascorbic acid, β-glycerophosphate, cholecalciferol and dexamethasone for at least 2 weeks. Before the seeding, collagenase type I (Gibco) solution (15 mg/ml) was applied for 20 min on an orbital shaker to promote cell matrix dissolution; then, cells were trypsinized for 10 min. Next, collagen gel with 750,000 cells/ml suspension was used to fill the gel ports. The cell suspension density was optimized by balancing the maximum effect induced by osteo-differentiated hBM-MSCs while limiting the possible gel degradation. Cells were cultured for 6 days before cancer cell injection in order to recreate an osteo-cell conditioned microenvironment (3 days supplemented with osteogenic medium, 3 days supplemented with endothelial cell medium). Red fluorescent protein (RFP)-transfected human umbilical vein endothelial cells (HUVECs) were commercially obtained (Angio-Proteomie) and cultured in endothelial growth medium (EGM-2MV; Lonza). According to a previously optimized cell seeding protocol [41], 40 μl HUVEC suspension at 2×10^6 cells/ml were introduced 3 days after seeding osteo-differentiated hBM-MSCs. All the experiments were conducted using HUVECs of passage 8 or lower. Human mammary adenocarcinoma cells MDA-MB-231 (American Type Culture Collection (ATCC)) were selected for high invasiveness and their ability to metastasize *in vivo* [50, 51]. Green fluorescent protein (GFP)-expressing MDA-MB-231 were cultured in standard Dulbecco's Modified Eagle Medium (DMEM; Invitrogen) supplemented with 10% Fetal Bovine Serum (FBS; Invitrogen), 1% L-glutamine and antibiotics, and were introduced 3 days after endothelial cell seeding by injecting 40 μl of 50,000 cells/ml cell suspension. The medium was replaced 1 h later with endothelial cell culture medium. All cultures were kept in a humidified incubator maintained at 37°C and 5% CO_2. Control experiments were performed with a collagen gel-only matrix, following the same protocol.

2.3. Immunofluorescent staining

Samples were washed with PBS and fixed with 4% paraformaldehyde (PFA) for 15 min at room temperature. Next, cells were washed twice with PBS and incubated with 0.1% Triton-X 100 solution for 5 min at room temperature. After washing twice with PBS, cells were blocked with 5% BSA + 3% goat serum solution for at least 3 h at 4°C. Vascular endothelial-cadherin (VE-cadherin) was labeled with rabbit polyclonal antibody (Abcam) at 1:100 dilution, Ki-67 was labeled with rabbit polyclonal antibody (Abcam) at 1:500 dilution, osteocalcin was labeled with rabbit polyclonal antibody (BTI) at 1:500 dilution, osteonectin was labeled with rabbit polyclonal antibody (Santa Cruz Biotechnology) at 1:60 dilution and osteopontin was labeled with rabbit polyclonal antibody (Abcam) at 1:100 dilution. Fluorescently-labeled secondary antibodies (Invitrogen) were used at 1:200 dilution. Cell nuclei were stained with 4'6-Diamidino-2-Phenylindole (DAPI; 5 mg/ml; Invitrogen) at 1:500 dilution while F-actin filaments were stained with AlexaFluor633 phalloidin (Invitrogen) at 1:100 dilution. If not differently specified, all the images were captured using a confocal microscope (Olympus IX81) and processed with Imaris software (Bitplane Scientific Software).

2.4. Conditioned assays: addition of CXCL5 and CXCR2 blocking agent

The cross-talk between MDA-MB-231 and osteo-differentiated hBM-MSCs was analyzed by investigating a signaling pathway involving the osteoblast-secreted inflammatory chemokine CXCL5 and the breast cancer cell surface receptor CXCR2 [52–54]. The selected chemokine was used to test the extravasation ability of breast cancer cells without the presence of an osteo-cell conditioned matrix while blocking experiments were performed

to quantify the extravasation rate of CXCR2-blockedcancer cells within the standard osteo-cell conditioned matrix. Recombinant human CXCL5/ENA-78 (R&D Systems) was diluted to 12 nM and added to the lateral media channels of collagen gel-only devices30 min before cancer cell seeding; fresh CXCL5-containing medium was replaced 1 h after the seeding and 12 h later to guarantee a stable gradient through the gel regions. In CXCR2 blocking experiments, cancer cells were incubated with 5 μg/ml mouse monoclonal antibody anti-CXCR2 (R&D Systems) 1h before the seeding; additionally, fresh antibody suspension was added 1h after the seeding to the central media channel of osteo-differentiated hBM-MSC-containing devices to saturate all cancer cell target receptors. Control experiments were performed by adding IgG antibody at the same CXCL5 or anti-CXCR2 concentrations, following identical protocols.

2.5. Extravasation and micrometastasis metrics

Confocal data were analyzed using Imaris software and its tracking algorithms for selecting and counting cell nuclei and GFP-derived signals within a specific region of interest (ROI). The ROI was defined as the 3D region between two PDMS walls, containing both the gel matrix and the endothelial monolayer interfacing the central media channel (Fig. 1B). The ROI dimensions were 250 μm × 250 μm × 150 μm (height) and each device contained 8 ROIs. The extravasation percentages were measured per device and subsequently averaged while the extravasation distance was quantified averaging data extracted from each specific condition as a single group. Extravasation events were observed using real time confocal microscopy (movie 1). According to our previous studies demonstrating that extravasation events mostly occur within the first 24 h, we quantified cell proliferation by counting the total number of cells per device at day 1, 2, 3 and 5. The number of cells per micrometastasis, the percentage of micrometastasis-positive ROIs and the number of micrometastases per ROI were computed.

3. Results and discussion

3.1. Generation of the osteo-cell conditioned microenvironment

The originality and relevance of the present work lie in the ability to specifically recreate an organ-specific tumor microenvironment by combining a well known biocompatible material, collagen gel type I, conditioned by bone-specific proteins secreted directly from primary human cells, thus modeling the extravasation process of breast cancer cells into an osteo-cell conditioned microenvironment. A key point of our system is that the extracellular matrix with secreted proteins from osteo-differentiated cells better mimics the complex cell signaling present in the *in vivo* environment, with naturally-formed gradients rather than imposed nutrition or chemokine gradients. Primary hBM-MSCs were obtained from bone marrow samples of patients undergoing hip arthroplasty and pre-differentiated in osteogenic medium for at least 14 days before being introduced into microfluidic devices. Fig. 1A shows a schematic of the developed assay: osteo-differentiated hBM-MSCs (brown) embedded in a collagen matrix were initially introduced into the gel channels, while RFP HUVECs (red) were seeded 3 days later within the central media channel to create a monolayer covering the channel walls and the gel-channel interfaces, thus generating an endothelium. At day 6 GFP MDA-MB-231 human breast cancer cells (green) were injected into the same cell channel and the extravasation rate promoted by the osteo-cell conditioned microenvironment was analyzed during the following 24 h.

High resolution confocal imaging shows that osteo-differentiated hBM-MSCs are homogeneously dispersed within the gel regions and extend their cytoplasmatic protrusions in the 3D microenvironment (Fig. 1B and C, movie 2). Samples stained for nuclei (4'6-Diamidino-2-Phenylindole (DAPI), blue) and F-actin (phalloidin, green) together with RFP-

HUVECs clearly highlight the endothelial monolayer generation on the gel-channel interface and the optimal distribution of osteo-differentiated hBM-MSCs within the collagen gel. The tight connections of endothelium are further confirmed with VE-cadherin staining of the monolayer (Fig. S4). hBM-MSCs produce calcium and secrete bone-marker proteins such as osteocalcin, as demonstrated by Alizarin Red-S assay and immunofluorescent staining, respectively. Calcium deposits (Fig. 1D and S1A) appear as darker regions within the osteo-cell conditioned microenvironment while osteocalcin (Fig. 1E and S2A, green) encloses actively secreting osteo-differentiated hBM-MSCs. Moreover, the expression of two additional bone markers, i.e. osteonectin and osteopontin, was evaluated within 2D flasks to provide complete evidence of osteogenic differentiation (Fig. S2C and D) [55–57]. Taken together, these findings confirm hBM-MSC osteogenic differentiation, thus providing the potential to better study the specific transendothelial migration of breast cancer cells into bone.

3.2. Extravasation of cancer cells in the osteo-cell conditioned microenvironment

Extravasation of cancer cells into the 6.0 mg/ml collagen type I gel matrix with and without osteo-differentiated hBM-MSCs is shown in Fig. 2. MDA-MB-231 cancer cells transmigrated across the endothelial monolayer covering the microchannel into the collagen gel whether the matrix contained osteo-differentiated hBM-MSCs or not. However, the average percentage of cancer cells extravasated in each ROI was significantly different comparing the abovementioned conditions. In collagen gel-only matrix, 37.6 ± 7.3% cancer cells extravasated, nearly identical to 38% extravasation rate previously reported in 2.0 mg/ml collagen gel, suggesting that matrix density alone is not a major factor [41]. With the addition of osteo-differentiated hBM-MSCs to the collagen gel, cancer cell extravasation rate increased to 77.5 ± 3.7% (Fig. 2A and B). Moreover, the extravasated cancer cells travelled significantly further into the matrix as compared to the collagen gel-only matrix. Indeed, the extravasation distance into the gel during the first 24 h was 50.8 ± 6.2 μm when osteo-differentiated hBM-MSCs were present, while cancer cells travelled 31.8 ± 5.0 μm in collagen alone (Fig. 2C and D), showing a similar migration behavior compared to 2.0 mg/ml collagen gels (25.9 ± 3.4 μm) and thus suggesting a minor influence of ECM density. If we define 40 μm (approximately twice the average length of a cancer cell and the mean distance travelled by the cells) as the threshold distance to distinguish between strongly and weakly migrating cancer cells, our data show that only 25% of extravasated cancer cells in the collagen gel-only condition were detected beyond the threshold while the rest remained close to the endothelial monolayer (Fig. 2C (i)). On the other hand, 45.8% of transmigrated cancer cells in the osteo-cell conditioned microenvironment were detected beyond the threshold (Fig. 2C (ii)), suggesting the presence of factors not only promote cancer cell transendothelial migration, but also migration within the matrix [53]. No significant modifications in the osteo-cell conditioned matrix were detected 24 h after cancer cell injection suggesting that extravasated cells do not alter the physical properties of the microenvironment in the observed time interval (Fig. S6).

To investigate the possibility that extravasation and migration behavior of breast cancer cells were influenced by structural changes in the ECM induced by the osteogenic differentiation of hBM-MSCs we performed experiments to compare collagen gel structure with or without osteo-differentiated hBM-MSCs. Confocal reflectance images did not show a clearly detectable difference in the matrix structure, suggesting the ECM remodeling was not the key factor affecting breast cancer cell migration (Fig. S5). However, we hypothesize a longer culture could induce changes in the structural properties and composition of the matrix, potentially influencing cancer cell behavior. Indeed, such changes in the microenvironment, characterized by secreting cells and active remodeling of the matrix

toward an even more physiological-like bone niche, could represent a significant improvement of the model.

3.3. Addition of CXCL5 and anti-CXCR2 - Effect on extravasation

As we found striking differences in extravasation of cancer cells in the two different microenvironments, we tried to investigate the effects of possible cytokines that are produced in the osteo-cell conditioned microenvironment on promoting extravasation. CXCL5 is one of the major chemokines that osteoblasts secrete and CXCR2 is a breast cancer cell surface receptor for this ligand. CXCL5 is known to activate Snail, a transcription factor involved in cancer cell invasiveness and migration [53]. Moreover, it has been demonstrated that Snail over-expression in breast cancer cells can up-regulate Axl expression, a tyrosine kinase receptor [52], which in turn is important for breast cancer cell extravasation [54]. Furthermore, the CXCR2 ligands CXCL5 and CXCL1 were recently shown to be secreted by mouse BM-MSCs and promote mammary cancer cell migration [58]. An enzymatic assay (CXCL5/ENA-78 enzyme-linked immunosorbent assay (ELISA)) confirmed the production of CXCL5 from osteo-differentiated hBM-MSCs at 3 weeks, showing a higher concentration (375 ± 1.65 pg/ml) compared to non-differentiated hBM-MSCs (162 ± 11.3 pg/ml) (Fig. S9A). No CXCL5 was detected within control osteogenic medium or endothelial cell medium. Moreover, immunofluorescent staining demonstrated the presence of CXCR2 surface receptor on MDA-MB-231 cells (Fig. S6B). Based upon these findings, we further investigated their role in extravasation (Fig. 3). Incubation of cancer cells with CXCR2 blocking antibody reduced extravasation in osteo-differentiated hBM-MSC-embedded collagen gel from $77.5 \pm 3.7\%$ to $45.8 \pm 5.4\%$, whereas incubation of cancer cells with control IgG had no significant effect on extravasation ($81.4 \pm 7.4\%$) (Fig. 3A and B). Moreover, the addition of CXCL5 ligand to collagen gel-only matrices led to an increase in the percentage of cancer cell extravasation from $37.6 \pm 7.3\%$ to $78.3 \pm 9.7\%$, while the addition of control IgG produced no significant effect ($25.7 \pm 16.7\%$) (Fig. 3C and D).

Interestingly, the distance that extravasated cancer cells travelled into the gel matrix after transmigration was significantly greater with the addition of CXCL5 compared to control collagen gel-only experiments (54.7 ± 5.8 μm vs. 31.8 ± 5.0 μm). However, blocking CXCR2 produced no effect on the distance travelled by extravasated cancer cells migrating into collagen gel embedded with hBM-MSCs compared to experiments performed with non-treated cancer cells (46 ± 5.7 μm vs. 50.8 ± 6.2 μm), suggesting that the role of CXCR2 in breast cancer cell migration within the bone tissue could be less critical compared to that of other receptors (Fig. 3E).

Several factors secreted *in vivo* by the bone microenvironment can promote the extravasation of breast cancer cells including CXCL12/SDF-1α [59] and CX3CL1/ fractalkine [60]. Although we did not investigate the specific role played by different molecules, our data show a significant difference when osteo-differentiated hBM-MSCs were embedded in the collagen matrix both in terms of extravasation rate and migration distance, thus highlighting the potential for organ-specific *in vitro* models to clarify features of different cancer types. To better characterize the effect of CXCL5 on breast metastatic cells we generated a gradient through a collagen gel-only matrix (Fig. S12), anticipating a critical role for this molecule in transendothelial migration and chemoattraction to bone.

3.4. Formation of micrometastases

Lethality of metastatic tumors depends on the formation of a metastatic niche, which develops when cancer cells extravasate into a secondary organ site and proliferate [2]. In our system, cancer cells were cultured up to 5 days after being introduced into the vessel-

mimicking channel, covered with an endothelial monolayer and adjacent to an osteo-cell conditioned collagen matrix embedded with osteo-differentiated hBM-MSCs. Our earlier results show that there was no significant difference in the percentage of ROIs containing extravasated cancer cells between day 1 and day 3 after their introduction (72% vs. 79%) [41]. While this seems to indicate that most cancer cells extravasate within the first 24 h of their introduction, the prolonged tri-culture allowed us to better characterize the behavior of cancer cells after extravasation, leading to colonization within the microenvironment, as seen in Fig. 4A and B. The extravasated cancer cells proliferated and formed micrometastases of various sizes ranging from 4 cells to more than 60 cells (Fig. 4C). We defined a cell cluster as a micrometastasis with at least 4 cancer cells either in direct contact or separated by less than one cell body length (assuming average cancer cell diameter ~20 μm), consistent with previous studies [18, 61]. The percentage of regions containing micrometastases was 48.4% (n=31 ROIs were analyzed in 5 independent devices). In total, 38 micrometastases were detected: 6 clusters contained at least 10 cells while 4 were constituted by more than 35 cells each (Fig. 4C). The number of cancer micrometastases per gel region was equally distributed among ROIs containing 1 to 4 micrometastases each (Fig. 4D). Notably, large micrometastases (>30 cells) tended to be found in isolation or associated with another small micrometastasis (Fig. S10).

The average number of cancer cells per device found within the gel regions was 13.8 at day 1, increasing to 17.8 and 34 at days 2 and 3, respectively, and reaching 132 at day 5 (Fig. S11). While it is possible that all cell types moved around in the system during the culture, it seems the increased number of cancer cells leading to the formation of clusters is primarily due to proliferation, since we observed the number of cancer cells increasing exponentially in each device during 5 days of culture. Moreover, all extravasated cancer cells were shown to be in active cell cycle within the new colonized microenvironment, as indicated by positive Ki-67 staining (Fig. 4A and B insets).

Several studies were previously reported to study the generation of metastases to bone and bone marrow. While these works provided much new insight into cancer cell-parenchyma cell interactions, they did not address the extravasation process itself. Mastro and Vogler adapted a bioreactor to grow multiple-cell-layer osteogenic tissues from osteoblast cell lines analyzing the ossification process over a time period up to 10 months. Breast cancer cells were added to tissues at different stages of phenotypic maturity and their ability to proliferate, generate microtumors and degrade the osteoblast-derived matrix were observed [62]. Lescarbeau and colleagues showed that paracrine factors secreted by hMSCs can increase prostate cancer cell survival while the interaction with a bone marrow-like ECM can lead to cancer cell morphological changes, chemoresistance and increased levels in the phosphorylation of proteins involved in cancer-related signaling pathways [63].

Overall, our data lead us to conclude that breast cancer cells found a receptive microenvironment that supported their growth, proliferation and formation of micrometastases. Extrapolating these results, a longer culture time could promote the generation of much more organized structures secreting chemokines and growth factors affecting the local microenvironment.

4. Conclusions

We have presented an advanced human organ-specific microfluidic 3D *in vitro* model to analyze the extravasation of highly metastatic breast cancer cells into an osteo-cell conditioned microenvironment. We have provided unique quantitative results concerning the interplay between a specific "seed and soil couple" by computing extravasation rate and extravasated distance of breast cancer cells in the presence of an attractive matrix.

Moreover, we have shown how the molecular pathway involving breast cancer cell surface receptor CXCR2 and bone-secreted chemokine CXCL5 plays a pivotal role in the extravasation process of breast cancer cells. Finally, we have observed that extravasated cancer cells can proliferate and generate micrometastases within the osteo-cell conditioned microenvironment, thus demonstrating the capabilities of the bone-specific model and paving the way to the generation of increasingly detailed assays to expand our knowledge of cancer biology and contribute to the development of more specific and effective anti-cancer treatments.

Supplementary Material

Refer to Web version on PubMed Central for supplementary material.

Acknowledgments

References

1. Chaffer CL, Weinberg RA. A perspective on cancer cell metastasis. Science. 2011; 331:1559–1564. [PubMed: 21436443]

2. Valastyan S, Weinberg RA. Tumor metastasis: molecular insights and evolving paradigms. Cell. 2011; 147:275–292. [PubMed: 22000009]

3. Chambers AF, Groom AC, MacDonald IC. Dissemination and growth of cancer cells in metastatic sites. Nat Rev Cancer. 2002; 2:563–572. [PubMed: 12154349]

4. Fidler IJ. The pathogenesis of cancer metastasis: the 'seed and soil' hypothesis revisited. Nat Rev Cancer. 2003; 3:453–458. [PubMed: 12778135]

5. Gupta GP, Massague J. Cancer metastasis: building a framework. Cell. 2006; 127:679–695. [PubMed: 17110329]

6. Hanahan D, Weinberg RA. The hallmarks of cancer. Cell. 2000; 100:57–70. [PubMed: 10647931]

7. Joyce JA, Pollard JW. Microenvironmental regulation of metastasis. Nat Rev Cancer. 2009; 9:239–252. [PubMed: 19279573]

8. Fukuda M, Hiraoka N, Yeh JC. C-type lectins and sialyl Lewis X oligosaccharides. Versatile roles in cell-cell interaction. J Cell Biol. 1999; 147:467–470. [PubMed: 10545492]

9. Miles FL, Pruitt FL, van Golen KL, Cooper CR. Stepping out of the flow: capillary extravasation in cancer metastasis. Clin Exp Metastasis. 2008; 25:305–324. [PubMed: 17906932]

10. Zipin A, Israeli-Amit M, Meshel T, Sagi-Assif O, Yron I, Lifshitz V, et al. Tumormicroenvironment interactions: the fucose-generating FX enzyme controls adhesive properties of colorectal cancer cells. Cancer Res. 2004; 64:6571–6578. [PubMed: 15374970]

11. Khatib AM, Auguste P, Fallavollita L, Wang N, Samani A, Kontogiannea M, et al. Characterization of the host proinflammatory response to tumor cells during the initial stages of liver metastasis. Am J Pathol. 2005; 167:749–759. [PubMed: 16127154]

12. Roussos ET, Condeelis JS, Patsialou A. Chemotaxis in cancer. Nat Rev Cancer. 2011; 11:573–587. [PubMed: 21779009]

13. Al-Mehdi AB, Tozawa K, Fisher AB, Shientag L, Lee A, Muschel RJ. Intravascular origin of metastasis from the proliferation of endothelium-attached tumor cells: a new model for metastasis. Nat Med. 2000; 6:100–102. [PubMed: 10613833]

14. Kebers F, Lewalle JM, Desreux J, Munaut C, Devy L, Foidart JM, et al. Induction of endothelial cell apoptosis by solid tumor cells. Exp Cell Res. 1998; 240:197–205. [PubMed: 9596992]

15. Paget S. The distribution of secondary growths in cancer of the breast. 1889. Cancer Metastasis Rev. 1989; 8:98–101. [PubMed: 2673568]

16. Bussard KM, Gay CV, Mastro AM. The bone microenvironment in metastasis; what is special about bone? Cancer Metastasis Rev. 2008; 27:41–55. [PubMed: 18071636]

17. Coleman RE. Skeletal complications of malignancy. Cancer. 1997; 80:1588–1594. [PubMed: 9362426]

18. Naumov GN, Wilson SM, MacDonald IC, Schmidt EE, Morris VL, Groom AC, et al. Cellular expression of green fluorescent protein, coupled with high-resolution in vivo videomicroscopy, to monitor steps in tumor metastasis. J Cell Sci. 1999; 112(Pt 12):1835–1842. [PubMed: 10341203]

19. Stoletov K, Kato H, Zardouzian E, Kelber J, Yang J, Shattil S, et al. Visualizing extravasation dynamics of metastatic tumor cells. J Cell Sci. 2010; 123:2332–2341. [PubMed: 20530574]

20. Goldstein RH, Weinberg RA, Rosenblatt M. Of mice and (wo)men: mouse models of breast cancer metastasis to bone. J Bone Miner Res. 2010; 25:431–436. [PubMed: 20200984]

21. Kuperwasser C, Dessain S, Bierbaum BE, Garnet D, Sperandio K, Gauvin GP, et al. A mouse model of human breast cancer metastasis to human bone. Cancer Res. 2005; 65:6130–6138. [PubMed: 16024614]

22. Florczyk SJ, Wang K, Jana S, Wood DL, Sytsma SK, Sham JG, et al. Porous chitosan-hyaluronic acid scaffolds as a mimic of glioblastoma microenvironment ECM. Biomaterials. 2013; 34:10143–10150. [PubMed: 24075410]

23. Kemppainen JM, Hollister SJ. Differential effects of designed scaffold permeability on chondrogenesis by chondrocytes and bone marrow stromal cells. Biomaterials. 2010; 31:279–287. [PubMed: 19818489]

24. Hendrix MJ, Seftor EA, Seftor RE, Fidler IJ. A simple quantitative assay for studying the invasive potential of high and low human metastatic variants. Cancer Lett. 1987; 38:137–147. [PubMed: 3690504]

25. Sagnella SM, Kligman F, Anderson EH, King JE, Murugesan G, Marchant RE, et al. Human microvascular endothelial cell growth and migration on biomimetic surfactant polymers. Biomaterials. 2004; 25:1249–1259. [PubMed: 14643599]

26. Uygur B, Wu WS. SLUG promotes prostate cancer cell migration and invasion via CXCR4/CXCL12 axis. Mol Cancer. 2011; 10:139. [PubMed: 22074556]

27. Kothapalli CR, Kamm RD. 3D matrix microenvironment for targeted differentiation of embryonic stem cells into neural and glial lineages. Biomaterials. 2013; 34:5995–6007. [PubMed: 23694902]

28. Nie FQ, Yamada M, Kobayashi J, Yamato M, Kikuchi A, Okano T. On-chip cell migration assay using microfluidic channels. Biomaterials. 2007; 28:4017–4022. [PubMed: 17583787]

29. Yang K, Han S, Shin Y, Ko E, Kim J, Park KI, et al. A microfluidic array for quantitative analysis of human neural stem cell self-renewal and differentiation in three-dimensional hypoxic microenvironment. Biomaterials. 2013; 34:6607–6614. [PubMed: 23777909]

30. Leclerc E, David B, Griscom L, Lepioufle B, Fujii T, Layrolle P, et al. Study of osteoblastic cells in a microfluidic environment. Biomaterials. 2006; 27:586–595. [PubMed: 16026825]

31. Chung S, Sudo R, Mack PJ, Wan CR, Vickerman V, Kamm RD. Cell migration into scaffolds under co-culture conditions in a microfluidic platform. Lab Chip. 2009; 9:269–275. [PubMed: 19107284]

32. Huang Y, Agrawal B, Sun D, Kuo JS, Williams JC. Microfluidics-based devices: New tools for studying cancer and cancer stem cell migration. Biomicrofluidics. 2011; 5:13412. [PubMed: 21522502]

33. Haessler U, Teo JC, Foretay D, Renaud P, Swartz MA. Migration dynamics of breast cancer cells in a tunable 3D interstitial flow chamber. Integr Biol (Camb). 2012; 4:401–409. [PubMed: 22143066]

34. Liu T, Li C, Li H, Zeng S, Qin J, Lin B. A microfluidic device for characterizing the invasion of cancer cells in 3-D matrix. Electrophoresis. 2009; 30:4285–4291. [PubMed: 20013914]

35. Sung KE, Yang N, Pehlke C, Keely PJ, Eliceiri KW, Friedl A, et al. Transition to invasion in breast cancer: a microfluidic in vitro model enables examination of spatial and temporal effects. Integr Biol (Camb). 2011; 3:439–450. [PubMed: 21135965]

36. Mak M, Reinhart-King CA, Erickson D. Elucidating mechanical transition effects of invading cancer cells with a subnucleus-scaled microfluidic serial dimensional modulation device. Lab Chip. 2013; 13:340–348. [PubMed: 23212313]

37. Zervantonakis IK, Hughes-Alford SK, Charest JL, Condeelis JS, Gertler FB, Kamm RD. Threedimensional microfluidic model for tumor cell intravasation and endothelial barrier function. Proc Natl Acad Sci U S A. 2012; 109:13515–13520. [PubMed: 22869695]

38. Song JW, Cavnar SP, Walker AC, Luker KE, Gupta M, Tung YC, et al. Microfluidic endothelium for studying the intravascular adhesion of metastatic breast cancer cells. PLoS One. 2009; 4:e5756. [PubMed: 19484126]

39. Chaw KC, Manimaran M, Tay EH, Swaminathan S. Multi-step microfluidic device for studying cancer metastasis. Lab Chip. 2007; 7:1041–1047. [PubMed: 17653347]

40. Heyder C, Gloria-Maercker E, Entschladen F, Hatzmann W, Niggemann B, Zanker KS, et al. Realtime visualization of tumor cell/endothelial cell interactions during transmigration across the endothelial barrier. J Cancer Res Clin Oncol. 2002; 128:533–538. [PubMed: 12384796]

41. Jeon JS, Zervantonakis IK, Chung S, Kamm RD, Charest JL. In vitro model of tumor cell extravasation. PLoS One. 2013; 8:e56910. [PubMed: 23437268]

42. Ma C, Wang XF. In vitro assays for the extracellular matrix protein-regulated extravasation process. CSH Protoc. 2008; 2008 pdb prot5034.

43. Shin MK, Kim SK, Jung H. Integration of intra- and extravasation in one cell-based microfluidic chip for the study of cancer metastasis. Lab Chip. 2011; 11:3880–3887. [PubMed: 21975823]

44. Zhang Q, Liu T, Qin J. A microfluidic-based device for study of transendothelial invasion of tumor aggregates in realtime. Lab Chip. 2012; 12:2837–2842. [PubMed: 22648473]

45. Roodman GD. Mechanisms of bone metastasis. N Engl J Med. 2004; 350:1655–1664. [PubMed: 15084698]

46. Mundy GR. Metastasis to bone: causes, consequences and therapeutic opportunities. Nat Rev Cancer. 2002; 2:584–593. [PubMed: 12154351]

47. Chung S, Sudo R, Vickerman V, Zervantonakis IK, Kamm RD. Microfluidic platforms for studies of angiogenesis, cell migration, and cell-cell interactions. Sixth International Bio-Fluid Mechanics Symposium and Workshop March 28–30, 2008 Pasadena, California. Ann Biomed Eng. 2010; 38:1164–1177. [PubMed: 20336839]

48. Shin Y, Han S, Jeon JS, Yamamoto K, Zervantonakis IK, Sudo R, et al. Microfluidic assay for simultaneous culture of multiple cell types on surfaces or within hydrogels. Nat Protoc. 2012; 7:1247–1259. [PubMed: 22678430]

49. Lopa S, Mercuri D, Colombini A, De Conti G, Segatti F, Zagra L, et al. Orthopedic bioactive implants: Hydrogel enrichment of macroporous titanium for the delivery of mesenchymal stem cells and strontium. J Biomed Mater Res A. 2013

50. Bos PD, Zhang XH, Nadal C, Shu W, Gomis RR, Nguyen DX, et al. Genes that mediate breast cancer metastasis to the brain. Nature. 2009; 459:1005–1009. [PubMed: 19421193]

51. Minn AJ, Gupta GP, Siegel PM, Bos PD, Shu W, Giri DD, et al. Genes that mediate breast cancer metastasis to lung. Nature. 2005; 436:518–524. [PubMed: 16049480]

52. Gjerdrum C, Tiron C, Hoiby T, Stefansson I, Haugen H, Sandal T, et al. Axl is an essential epithelial-to-mesenchymal transition-induced regulator of breast cancer metastasis and patient survival. Proc Natl Acad Sci U S A. 2010; 107:1124–1129. [PubMed: 20080645]

53. Hsu YL, Hou MF, Kuo PL, Huang YF, Tsai EM. Breast tumor-associated osteoblast-derived CXCL5 increases cancer progression by ERK/MSK1/Elk-1/Snail signaling pathway. Oncogene. 2013; 32:4436–4447. [PubMed: 23045282]

54. Vuoriluoto K, Haugen H, Kiviluoto S, Mpindi JP, Nevo J, Gjerdrum C, et al. Vimentin regulates EMT induction by Slug and oncogenic H-Ras and migration by governing Axl expression in breast cancer. Oncogene. 2011; 30:1436–1448. [PubMed: 21057535]

55. Chung EJ, Chien KB, Aguado BA, Shah RN. Osteogenic potential of BMP-2-releasing self-assembled membranes. Tissue Eng Part A. 2013 Available from URL: http://online.liebertpub.com/doi/abs/10.1089/ten.TEA.2012.0667.

56. Huang C, Ogawa R. Effect of hydrostatic pressure on bone regeneration using human mesenchymal stem cells. Tissue Eng Part A. 2012; 18:2106–2113. [PubMed: 22607391]

57. Perez RA, Kim M, Kim TH, Kim JH, Lee JH, Park JH, et al. Utilizing core-shell fibrous collagenalginate hydrogel cell delivery system for bone tissue engineering. Tissue Eng Part A. 2013 Available from URL: http://online.liebertpub.com/doi/abs/10.1089/ten.TEA.2013.0198.

58. Halpern JL, Kilbarger A, Lynch CC. Mesenchymal stem cells promote mammary cancer cell migration in vitro via the CXCR2 receptor. Cancer Lett. 2011; 308:91–99. [PubMed: 21601983]

59. Muller A, Homey B, Soto H, Ge N, Catron D, Buchanan ME, et al. Involvement of chemokine receptors in breast cancer metastasis. Nature. 2001; 410:50–56. [PubMed: 11242036]

60. Jamieson-Gladney WL, Zhang Y, Fong AM, Meucci O, Fatatis A. The chemokine receptor CX(3)CR1 is directly involved in the arrest of breast cancer cells to the skeleton. Breast Cancer Res. 2011; 13:R91. [PubMed: 21933397]

61. Cserni G, Bianchi S, Vezzosi V, van Diest P, van Deurzen C, Sejben I, et al. Variations in sentinel node isolated tumour cells/micrometastasis and non-sentinel node involvement rates according to different interpretations of the TNM definitions. Eur J Cancer. 2008; 44:2185–2191. [PubMed: 18691877]

62. Mastro AM, Vogler EA. A three-dimensional osteogenic tissue model for the study of metastatic tumor cell interactions with bone. Cancer Res. 2009; 69:4097–4100. [PubMed: 19435905]

63. Lescarbeau RM, Seib FP, Prewitz M, Werner C, Kaplan DL. In vitro model of metastasis to bone marrow mediates prostate cancer castration resistant growth through paracrine and extracellular matrix factors. PLoS One. 2012; 7:e40372. [PubMed: 22870197]
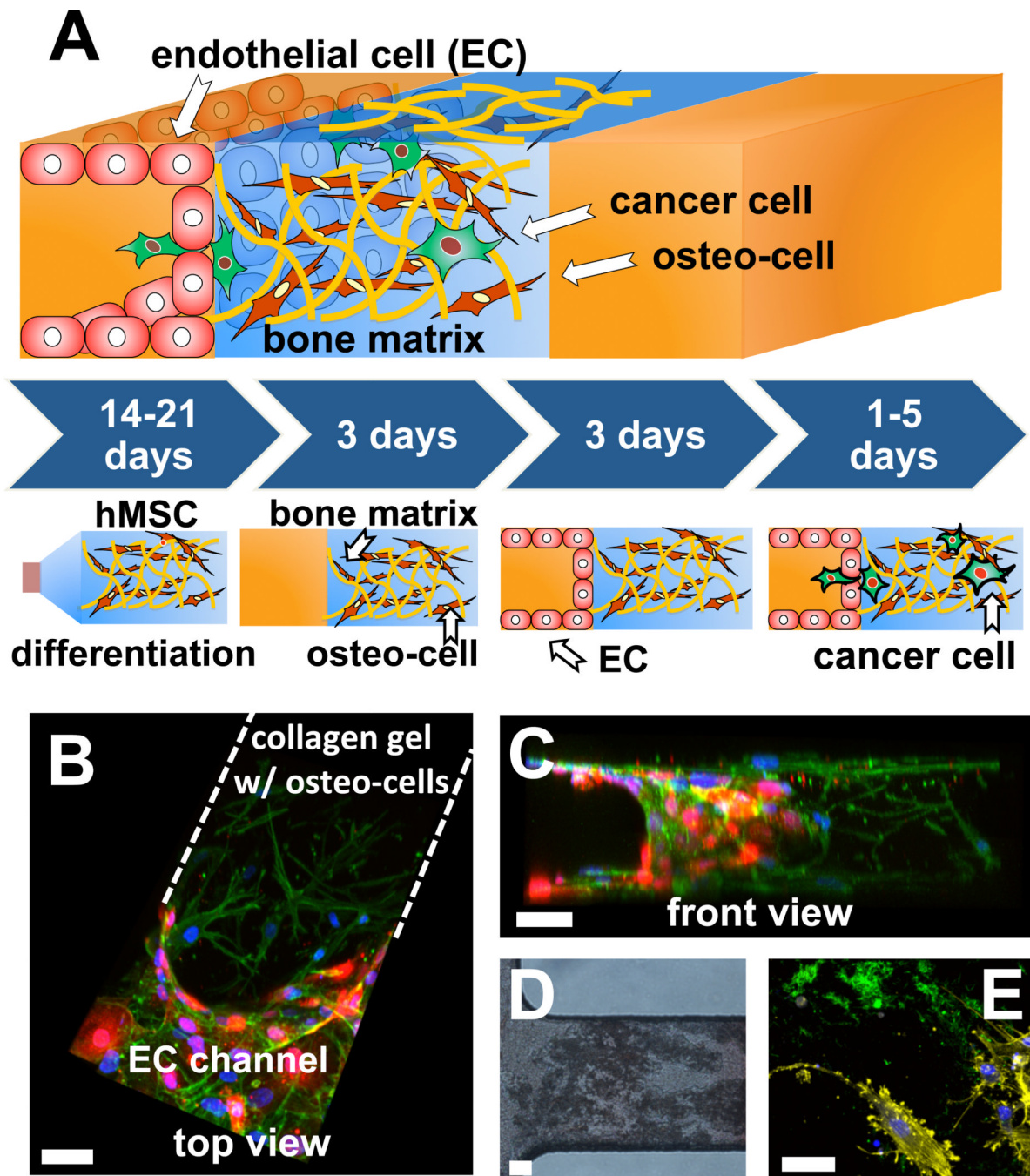
Fig. 1.
Generation of the osteo-cell conditioned microenvironment. (A) hBM-MSCs (brown) were cultured for 2–3 weeks within osteogenic medium and seeded within microfluidic devices where they started depositing extracellular matrix (yellow filaments). After 3 days endothelial cells (ECs) (red) were seeded and a monolayer covering the media channel was generated. Finally, cancer cells (green) were introduced after 3 additional days and their extravasation ability and micrometastasis generation were monitored for 1 to 5 days. (B and C) Three-dimensional reconstruction of a confocal stack represents a top (B) and a front view (C) of a single ROI. HUVECs (RFP) completely covered the channel walls while osteo-differentiated hBM-MSCs were homogeneously distributed within the collagen gel.

Cells were stained with DAPI (nuclei, blue) and phalloidin (F-actin, green). (D) Alizarin Red staining of calcium deposits (dark region) within a gel channel (optical microscopy, bright field). (E) Two-dimensional projection of a confocal stack highlights the ability of osteo-differentiated hBM-MSCs to secrete osteocalcin (green) within a 3D microenvironment. Cells were stained with DAPI (nuclei, blue) and phalloidin (F-actin, yellow). Osteo-differentiated hBM-MSCs are labeled as osteo-cells. Scale bars: 50 μm.
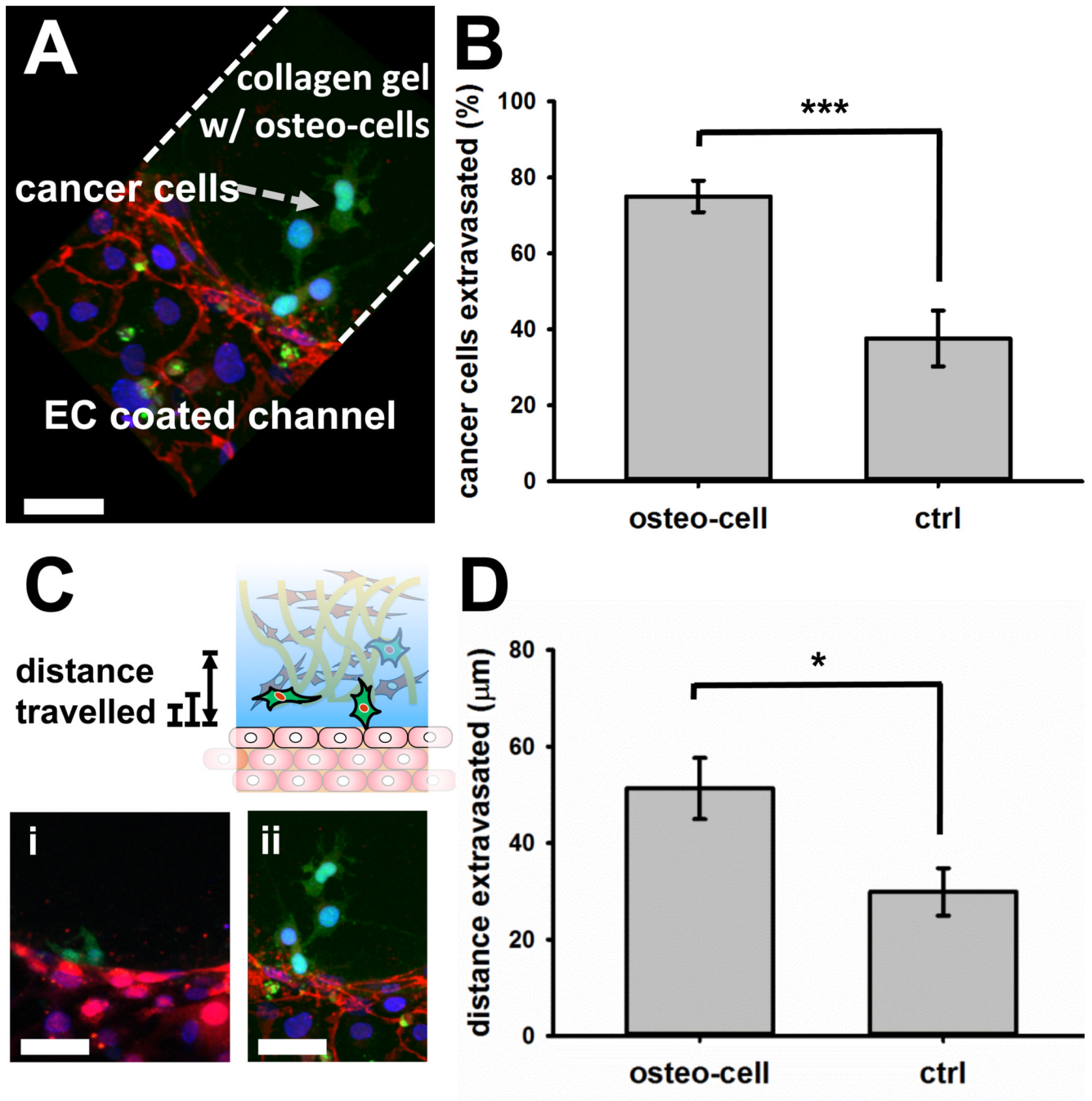
Fig. 2.
Extravasation of cancer cells into the collagen gel matrix with and without osteo-differentiated hBM-MSCs (labeled as osteo-cells). (A) Three-dimensional confocal reconstruction shows MDA-MB-231 cancer cells (GFP) transmigrated across the endothelial monolayer into the collagen gel containing osteo-differentiated hBM-MSCs. VE-cadherin (red) and DAPI (nuclei, blue) staining. (B) Average percentage of extravasated cancer cells was significantly higher (n=27(min)-39(max) regions, p<0.005) in the collagen gel with osteo-differentiated hBM-MSCs. (C) Projected images show extravasated cancer cells (GFP) travelled farther into the osteo-cell conditioned microenvironment (ii) compared to the collagen gel-only matrix (i). Cells were stained with (i) DAPI (nuclei, blue) and (ii) VE-

cadherin (red) + DAPI (nuclei, blue). HUVECs were RFP labeled. (D) Average distance travelled by extravasated cells into the gel matrix increased significantly in osteo-cell conditioned microenvironment (n=11(min)-17(max) regions, $p<0.05$). Scale bars: 50 μm.
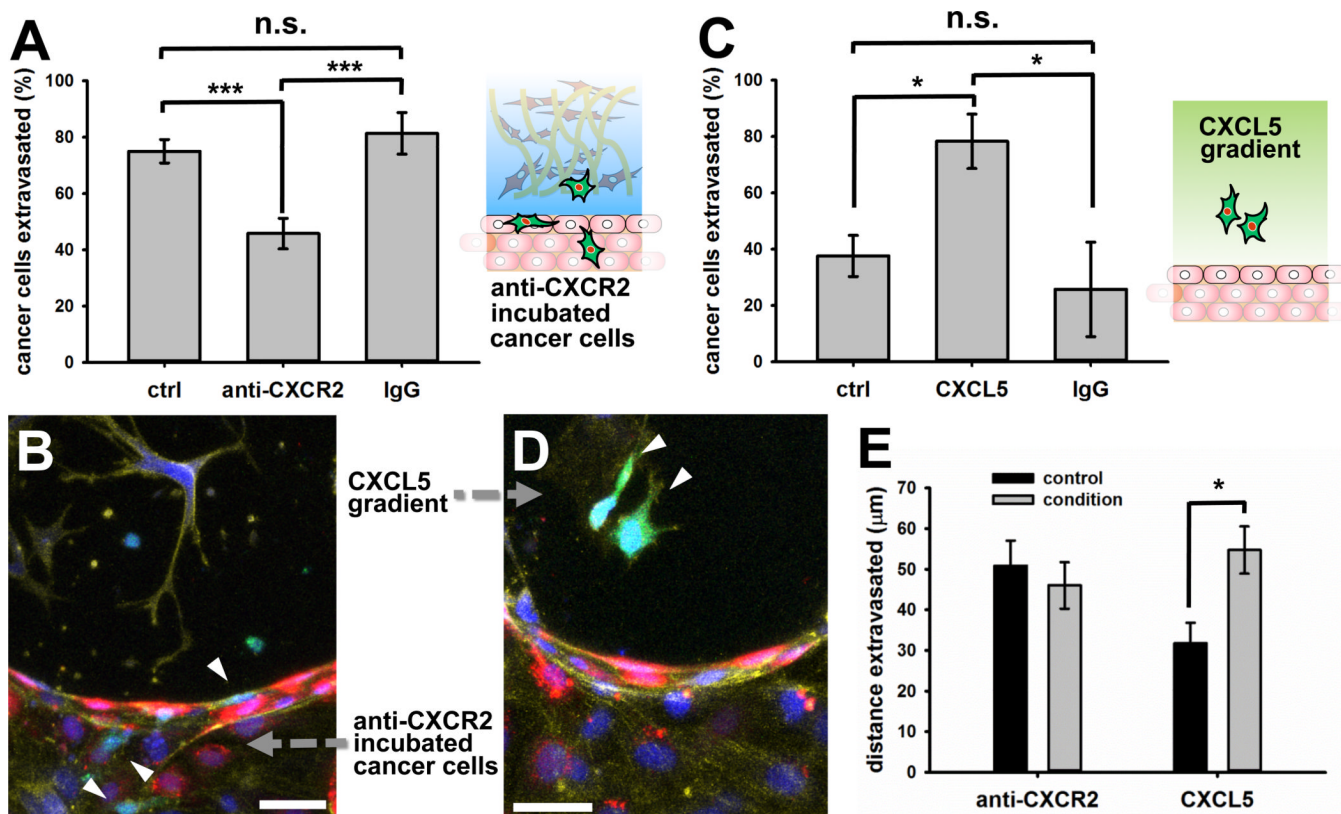
Fig. 3.
Effect of CXCL5 and CXCR2 in cancer cell extravasation. (A) Addition of CXCR2 blocking antibody significantly reduced cancer cell average extravasation within collagen gel containing osteo-differentiated hBM-MSCs compared to non-treated cancer cells (ctrl) or IgG incubated cancer cells (n=9(min)-24(max) regions, p<0.005). (B) Two-dimensional projection of a confocal stack shows that cancer cells (GFP, white arrows) generally remained within the endothelial cell (RFP)-coated channel and did not extravasate into the collagen gel containing osteo-differentiated hBM-MSCs when anti-CXCR2 antibody was added. Cells were stained with DAPI (nuclei, blue) and phalloidin (F-actin, yellow). (C) Addition of CXCL5 within collagen gel-only devices significantly enhanced the average percentage of cancer cell extravasation compared to unconditioned devices (ctrl) and addition of IgG (n=9(min)-24(max) regions, p<0.05). (D) Two-dimensional projection of a confocal stack showing two extravasated cancer cells (GFP, white arrows) inside CXCL5-conditioned collagen gel-only devices. Cells were stained with DAPI (nuclei, blue) and phalloidin (F-actin, yellow). HUVECs were RFP labeled. (E) The average extravasation distance was significantly higher with the addition of CXCL5 (condition) within collagen gel-only devices compared to unconditioned devices (p<0.05) whereas there was no significant difference within a osteo-cell conditioned matrix with (condition) or without (control) cancer cell incubation in CXCR2 blocking antibody (n=11(min)-17(max) regions). Scale bars: 50 μm.
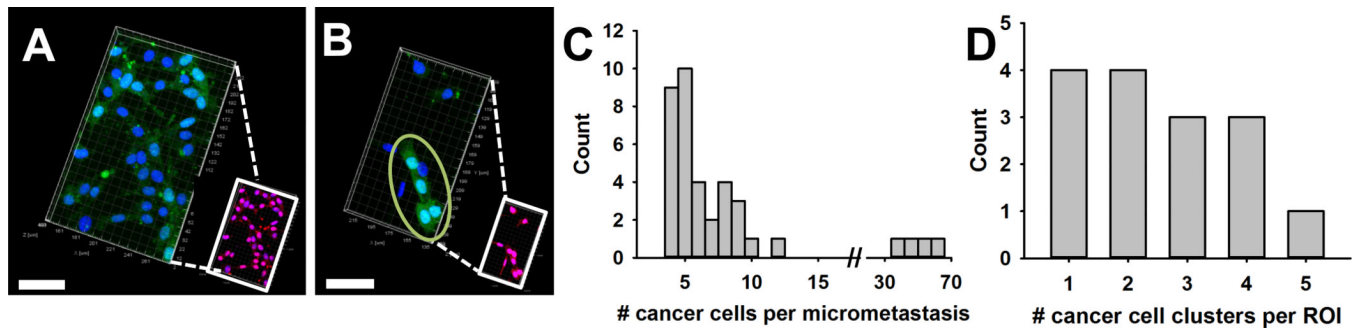
Fig. 4.
Generation of micrometastases within the osteo-cell conditioned microenvironment. Three-dimensional confocal images of a single gel region show a representative large (A) and small (B) cancer cell (GFP) micrometastasis. Ki-67 staining (red) demonstrates all cancer cells were proliferating within the colonized microenvironment. Cells were stained with DAPI (nuclei, blue). (C) Histogram showing micrometastasis distribution. Although 4 large clusters (>35 cells) were detected, micrometastases generally contained fewer than 10 cells. (D) Histogram represents the number of micrometastases per gel region (n=15 regions). Scale bars: 50 μm.